RECENT DEVELOPMENTS RELATED TO A CONVOLUTION-TYPE, PHASE-RESOLVING WAVE MODEL

Hemming A. Schäffer[1]

This paper shows some 2DV examples of recent advances related to the long-term, ongoing development of an elaborate, fully dispersive and highly nonlinear 3D phase resolving wave model based on the convolution-type approach. Using impulse response functions pre-computed by solving local Laplace problems the model is entirely explicit in space during the evolution in time. The explicit convolution integral involves only the near field surface variables and eliminates the need for solving global systems of equations. The first example is a linear random-wave application to wavemaker performance in a flume with a cavity behind an elevated generator and illustrates the capability of the model to handle complex geometry. The second example demonstrates the ability to generate and propagate highly nonlinear regular waves starting with transients entering still water. The third example concerns highly nonlinear regular deep-water waves and shows how the surface variables can be post-processed to provide the internal wave kinematics throughout the water column all the way to the free surface.

Keywords: wave transformations, convolution, nonlinearity, wave kinematics, wave generation, full dispersion

INTRODUCTION

The convolution-type wave model is under continuous development to meet the ambition of modeling nonlinear, fully dispersive, irregular, multidirectional waves as they transform over several kilometers of arbitrary bathymetry and interact with fixed or floating structures in complex-shaped domains. Various advancements in this direction can be found in papers by the author, see e.g. http://www.schafferwaves.dk/publications/.

The model relies on the commonly adopted time stepping of the kinematic and dynamic boundary conditions expressed directly in the free-surface variables. This requires a kinematics closure essentially providing the vertical surface velocity in terms of the horizontal ditto, and this is where the model stands out by realizing the closure as an explicit procedure involving a convolution integral and pre-computed, locally determined, impulse response functions. These functions show exponential horizontal decay and computing them involves the solution of the Laplace equation in local sub-domains extending just several water depths away from the impulse. For sub-domains that are horizontally open and have constant or mild-slope depth, the impulse response functions are available analytically. Nonlinearity is handled by adapting the perturbation scheme (Schäffer, 2008) of the high-order spectral method (West et. al., 1987, Dommermuth and Yue, 1987).

Although the general model development is targeting 3D applications, the present paper presents three 2DV examples showing various aspects of recent model developments. The first is related to complex geometry and is taken from a linear-wave application to the performance of an elevated piston-type wavemaker in a wave-current flume. The second example shows the ability of the model to propagate highly nonlinear waves of constant form. Although this is not really a new model feature, it makes up a suitable transition to the third example, which shows how the surface variables can be post-processed to obtain the internal wave kinematics of a highly nonlinear wave.

The name of the numerical model holding the specific implementation of the convolution approach is SWIFT (Surface Waves, Integral Fast Transformation) as referenced in some of the plot legends below.

WAVEMAKER APPLICATION

Wavemakers in physical test basins and flumes are typically designed using linear, analytical transfer functions between paddle motion and wave elevation. The underlying theoretical framework, however, only supports basic wavemaker types. Driven by the need to estimate the wave generation capabilities of a more complex wavemaker setup in a wave-current flume, the convolution wave model was generalized to account for wavemaker boundary conditions. The required pre-processing effort involved the numerical, evanescent solution to the 2D vertical Laplace equation in the near field of the wavemaker. This solution provided the necessary contribution to the impulse response functions of the convolution method. Next, the evolution of the wave field in time and space was computed as usual i.e. time-stepping the free-surface boundary conditions while applying the convolution for the surface

[1] SchäfferWaves, Sortedam Dossering 59D st, DK-2100 Copenhagen Ø, Denmark

kinematics closure, where the convolution essentially provides the vertical surface velocity from the horizontal one.

Running the model with a band-limited which noise wavemaker signal and relating that signal to the computed far-field surface elevation provided the desired wavemaker transfer function. Trials for the classical (elevated) piston-type wavemakers with analytically known transfer functions demonstrated the viability of the approach, which was subsequently used in support of the design of a more complex wavemaker setting.

Flume layouts considered

Four flume layouts were considered. These were all equipped with an elevated piston-type wavemaker of draft 0.5m on a constant water depth of 2.7m.

1. The first layout had a vertical wall directly underneath the mean position of the wavemaker, see Figure 1, top panel. This represents a standard setup, and linear wavemaker theory provides for an analytical result for the Biésel transfer function (H/S vs f, where H is the nominal wave height that can be generated with at wavemaker stroke, S, at frequency f).
2. The second layout had a cavity under the wavemaker and the vertical wall was located at a horizontal distance of one water depth behind the wavemaker front, see Figure 1, second panel from the top. No analytical wavemaker theory is available for this and the following layouts.
3. The third layout, Layout 3, represents the complexity of the actual flume and includes a shelf under the elevated piston. The shelf extends 0.40m from the mean position of the wavemaker front.
4. The fourth layout, Layout 4, is identical to Layout 3 except for the shelf, which now extends only 0.1m from the mean position of the wavemaker front. The reason for introducing Layout 4 will be given in the results section.

Numerical impulse response results

The basis for the time evolution is the set of impulse response functions. These decay exponentially with the horizontal distance from the impulse. The impulse response functions are split into a free-space component and a boundary adaptation component. Here free space refers to the horizontal direction and boundary adaptation refers all solid-wall boundaries except the bottom, for which no adaptation is needed. For constant depth, the free-space component is given analytically, see e.g. Schäffer (2009). For vertical-wall boundaries, including the simple layout with an elevated piston, the boundary adaptation component may also be evaluated analytically using imaging. This eliminates the need for a discrete Laplace solver. Applying the fully analytical impulse response functions during the time evolution and analyzing the resulting surface elevation time series results in an excellent match with linear wavemaker theory. However, the imaging technique is not available for more complex boundaries and to test the four layouts of Figure 1 on equal terms, the discrete Laplace solver has been used in all layouts for obtaining the boundary adaptation component. The use of the discrete Laplace solver introduces a slight loss of accuracy.

Figure 2 compares the total impulse response function for the four layouts in case of an impulse located at the still water level 0.95m from the wavemaker. To enhance small values the contours are plus/minus (4,1,1/4,1/16,1/64,1/256,1/1024,1/4096). The 1/4096 contour line comes close to the solid boundaries, where the response must vanish. Although the response adapts to the four different layouts, the responses at the still water level are almost identical. Since it is only the response at the still water level that enters the time-evolution procedure and affects the generated wave elevation, this example indicates that the layout has little influence on the wave generation capability.

Boundary conditions

Solid boundaries are modeled as impermeable walls with slip conditions. This applies to all boundaries except the free surface. Near the down-wave end of the flume, wave absorption is provided by a numerical sponge layer. In line with linear wavemaker theory, the wavemaker is modeled by specifying the instantaneous, horizontal paddle velocity at the mean position of the wavemaker front.

Wavemaker control signal and analysis procedure

The wavemaker signal was synthesized from a white-noise spectrum bounded by a frequency of f = 2.5Hz (kh = 68!) using the inverse FFT method. The periodicity of the synthesized input wave signal was $8192\Delta t = 163.84$s ($\Delta t = 0.02$s) and the model was run for twice this duration. The first half was taken as a warm-up period and the other half was analyzed by FFT. Provided the warm-up period is sufficient, the data to be analyzed are periodic and fit exactly into the FFT with no spectral leakage and no spectral variance. The raw spectra turn out smooth. The Biésel transfer function was determined as

the ratio between the respective amplitude spectra of the surface elevation at some distance from the wavemaker and the wavemaker control signal. The results were not sensitive to the chosen distance, provided it was long enough to keep clear of the local evanescent-mode field in the wavemaker vicinity.

Numerical wave generation results and discussion

The top panel of Figure 3 compares the computed Biésel transfer function for the upper two flume layouts of Figure 1 with the analytical solution for the simplest case. Before discussing the details, the overall result is clearly that all three results are very close. If fact they are so close that no physical model test would likely be able to detect the difference.

Looking a little closer at the results in Figure 3 (top panel), we first compare the numerical (blue) result with the theoretical (green) result for the simple layout with a wall beneath the wavemaker front. The influence of the wall on the impulse response functions was determined by a Laplace solver using a low-order finite difference scheme. A closer match (not shown) has been obtained by surpassing the Laplace-solver while taking in the wall effect through an image method. This indicates that the main reason for the slight deviations between blue and green lines in Figure 3 (top panel) is due to the limited accuracy of the Laplace-solver. This was confirmed by another test (not shown) in which the Laplace solver was run with a courser resolution resulting in the same trend of deviation, but to larger extent. Since the limitation of the Laplace solver has similar effects on the two layouts (comparing red and blue in Figure 3, top panel), the numerical model is expected to capture the difference between the two quite well. The difference is a few percent at maximum and may be either positive or negative.

Turning to Layout 3, results are shown in Figure 3, bottom panel, blue line. The deviation from the idealized case ‘Wall under WM’ (layout from top panel of Figure 1) is now appreciable. The largest performance loss is almost 11% and it occurs at a frequency slightly below 0.9Hz. In search for a possible explanation, the dispersion relation was evaluated at the shelf depth of 0.5m for a frequency of 0.97Hz resulting in a wavelength of 1.60m. Thus a quarter wavelength equals the shelf length of 0.4m and indicates that the performance loss might be due to negative interference between waves emitted directly from the wavemaker and waves re-reflected from the wavemaker after being reflected from the abrupt depth change at the tip of the shelf. The reason why the maximum performance loss occurs near 0.9Hz although the quarter wavelength case appears at 0.97Hz might be that an expected increase of reflections from the step at lower frequencies is more important than exact phasing of the crest-trough cancellation of negative interference.

To confirm the conjecture that it is the presence of the shelf rather than the specific layout of the cavity that matters, Layout 4 (Figure 1, bottom panel) was introduced. This layout is identical to Layout 3 except the shelf is shortened from 0.4m to 0.1m. The red line in the bottom panel of Figure 3 now shows a much closer resemblance with the simple layouts than Layout 3. For Layout 4, the performance loss has almost vanished.

With regard to the general accuracy of the numerical model results, improvements could likely be obtained by increasing the spatial resolution or the order of the Laplace solver used for the determination of the impulse response functions. Other options that might further improve the numerical exercise include enhancing the numerical sponge layer and/or involving a reflection analysis of the results. However, the quality of the results already appears to be satisfactory and there does not seem to be much point in pursuing these refinements.

Winding up, the cavity itself under the elevated piston-type wavemaker appears to have only a very small effect on the wave generation capability. However, Layout 3 (third panel of Figure 1) reduces the wave height that can be generated by up to 11% near a frequency of 0.9Hz. Hypothesizing that (relative to the schematic second layout in Figure 1) the shelf rather than the cavity change is the cause of this reduction, Layout 4 (bottom panel of Figure 1) with a shortened shelf was introduced. This shelf shortening almost eliminated the loss of wave generation performance and confirmed that the appreciable loss for Layout 3 is due to the shelf, while the specific layout of the cavity has little effect.

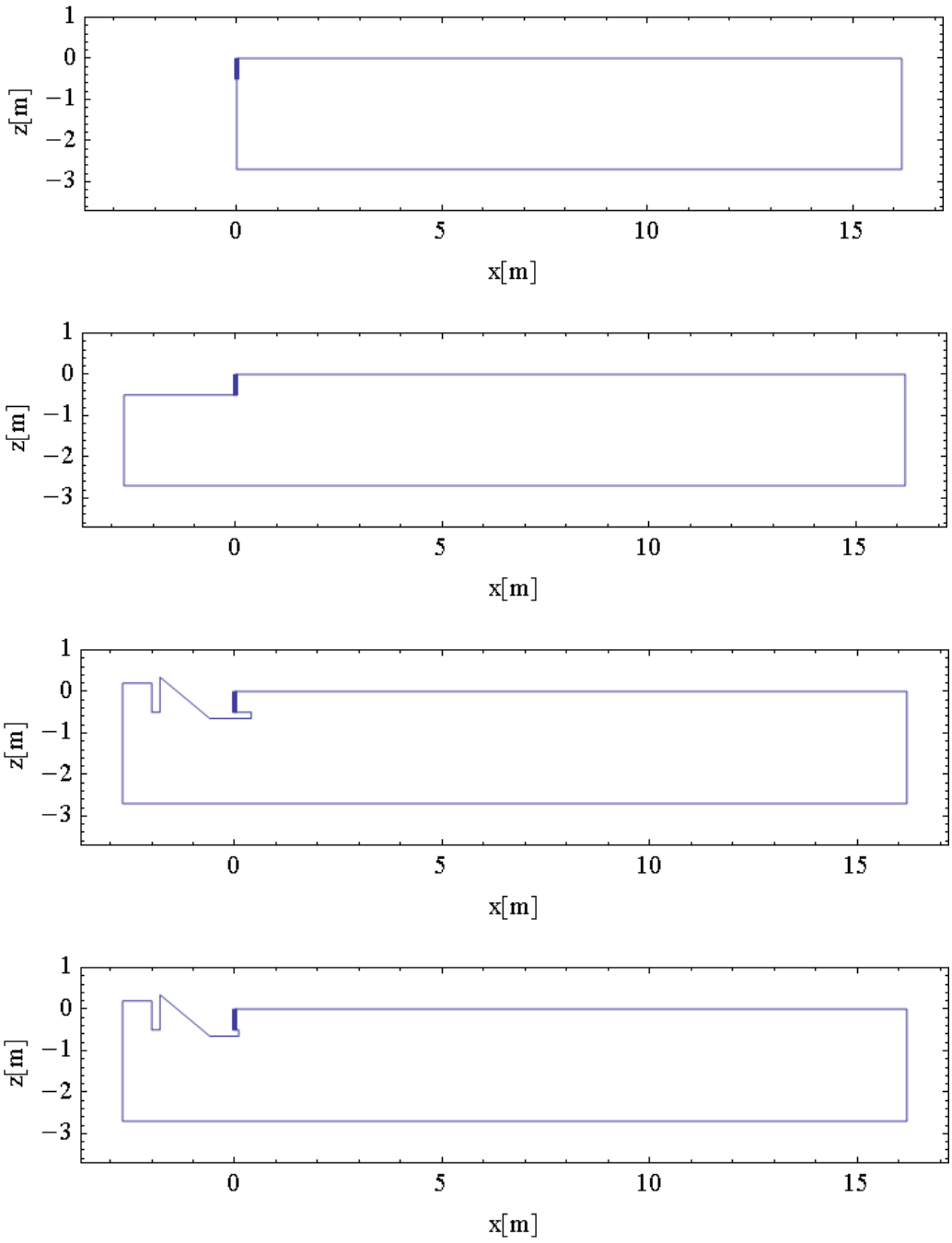

Figure 1. Wave flume layouts with elevated piston wavemaker of draft 0.5m on a depth of 2.7m. The thick short vertical line shows the wavemaker front. Top panel: Standard layout with wall under the wavemaker. Second panel: This layout has a cavity under the wavemaker. Third panel: Layout 3. Bottom panel: Layout 4 with shortened shelf.

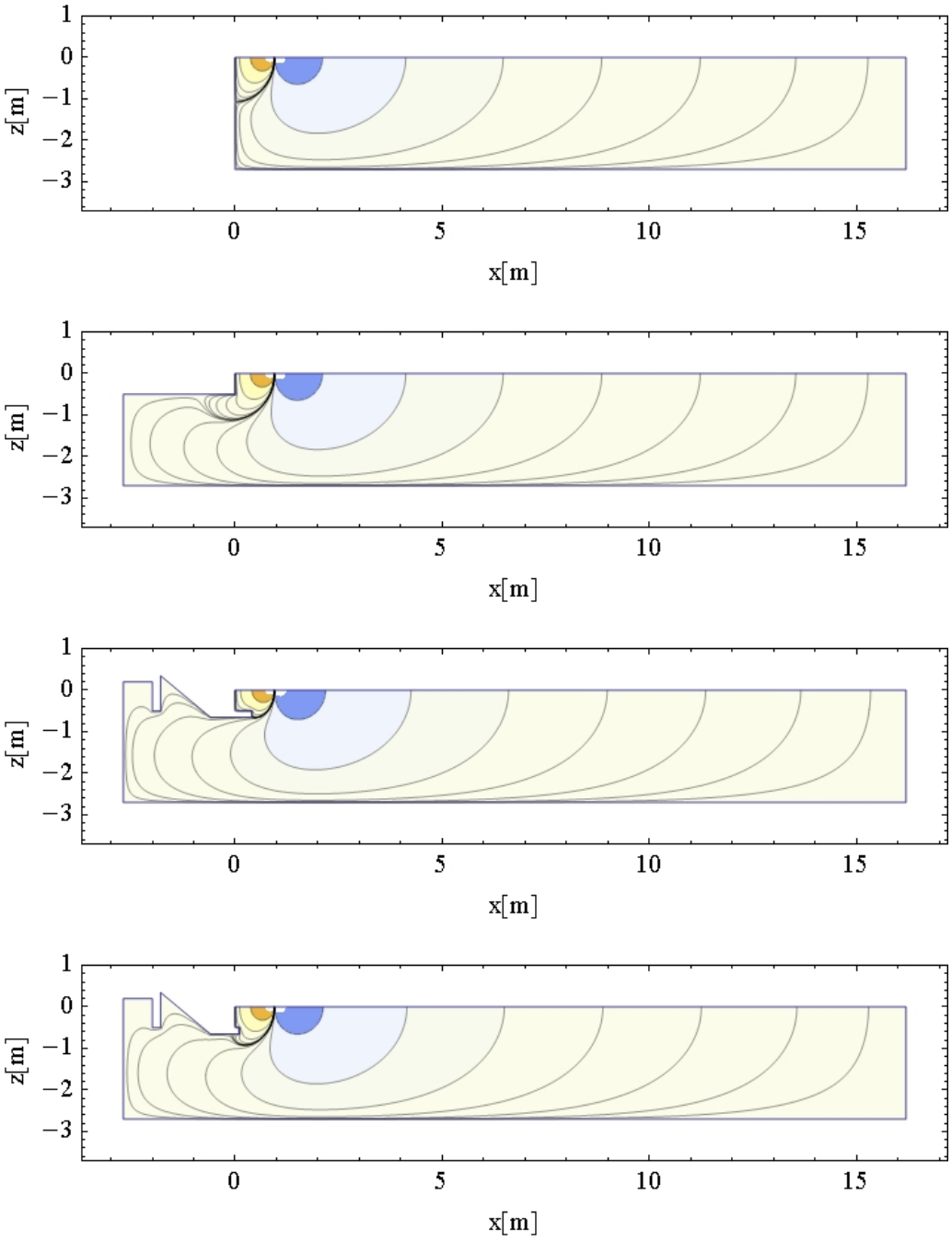

Figure 2. Contours of response to an impulse in the horizontal velocity at still water level at 0.95m from the wavemaker. The response decays exponentially in the horizontal direction. Contour values are plus/minus (4,1,1/4,1/16,1/64,1/256,1/1024,1/4096) with the smallest contours near the solid boundaries, where the impulse response vanishes. The four panels correspond to the four layouts of Figure 1.

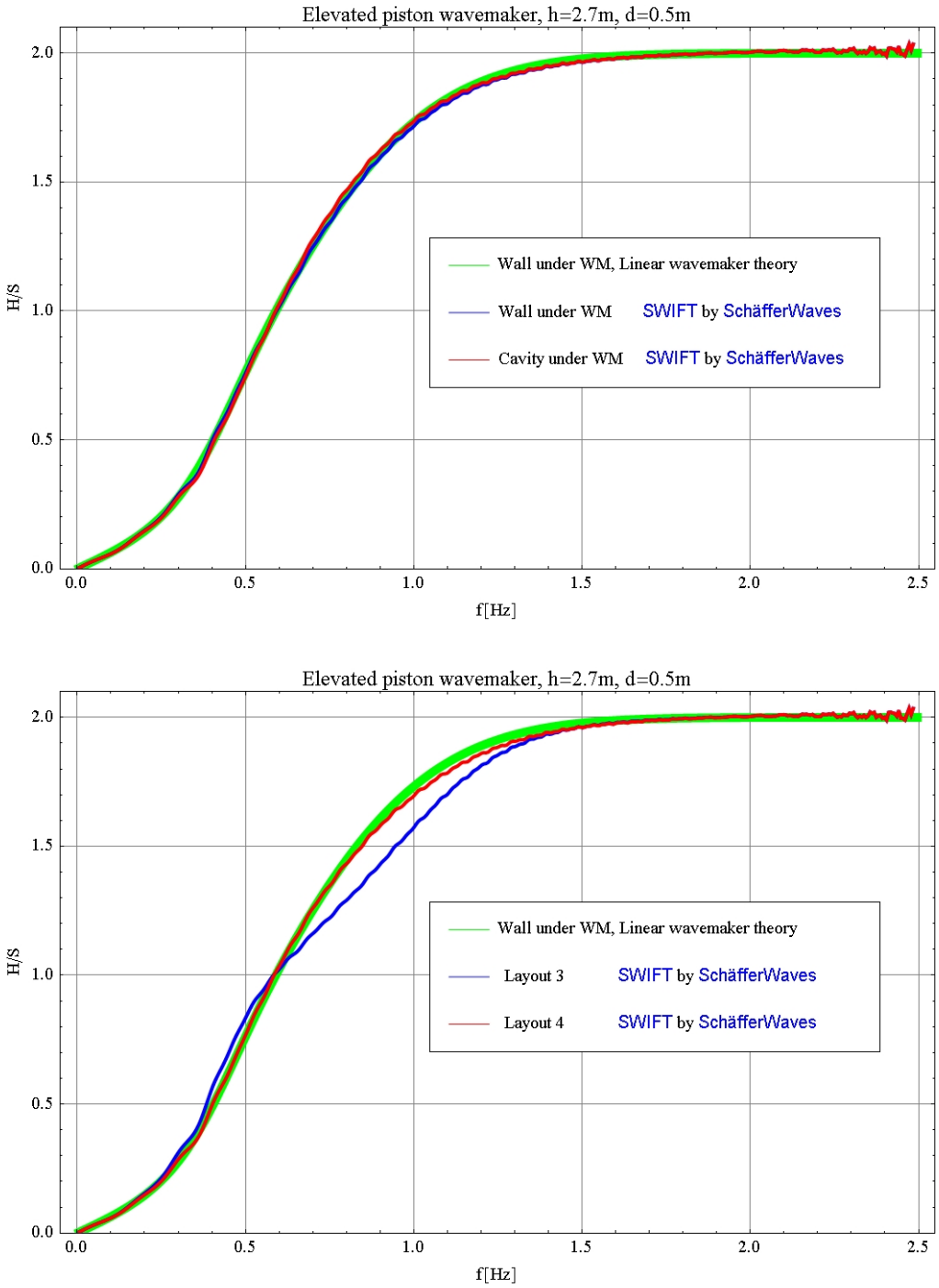

Figure 3. Biésel transfer function for the four wave flume layouts. Both panels show the theoretical result for the first layout in Figure 1 as reference (green line). Top panel: First two layouts in Figure 1. Bottom panel; Last two layouts in Figure 1.

PROPAGATION OF HIGHLY NONLINEAR WAVES

While the previous example concentrated on the numerical modeling of waves in a physical wave flume, the focus is now shifted towards a 2DV numerical setup better suited for the controlled modeling of nonlinear waves. Waves are generated to the far left in a relaxation zone and absorbed to the far right in an absorption zone (Bingham and Agnon, 2005). Stream Function Wave Theory for a highly

nonlinear wave (Rienecker and Fenton, 1981) provides the input for the wave generation in the relaxation zone in time and space and while this signal is ramped up in time, wave transients enter the initially quiescent water in the main section of the numerical domain. These waves carry a set-down of the mean water level, a feature which is not included in the usual Stream Function Wave Theory. To align the numerical situation with the theory, the initial water level in the numerical model was raised slightly.

While taking the average volume flux to zero, the wave of choice had a height of H = 0.258m, a period of T = 1.36s and the depth was h = 0.5m throughout. This corresponds to a wave in the intermediate depth range (L = 2.62m giving kh = 1.20) with a steepness of about 84% of the breaking limit. Considering this as a down-scaled prototype situation this could have been a traditional design wave for an offshore structure e.g. with H = 25.8m and T = 13.6s on h = 50m using a length scale of 1:100.

Figure 4 shows the computed surface elevation on top of the Stream Function Solution with the top panel showing a snap shot during the transient evolution, while the bottom panel shows the fully developed situation. The reminiscence of the slightly elevated initial water level is seen to the far right in the absorption zone. The crest heights are slightly jumpy during the transient phase (Figure 4, top panel), which is to be expected even under ideal circumstances. The final match with the reference solution is excellent (Figure 4, bottom panel) and indicates that the solution makes a good starting point for computing internal kinematics.

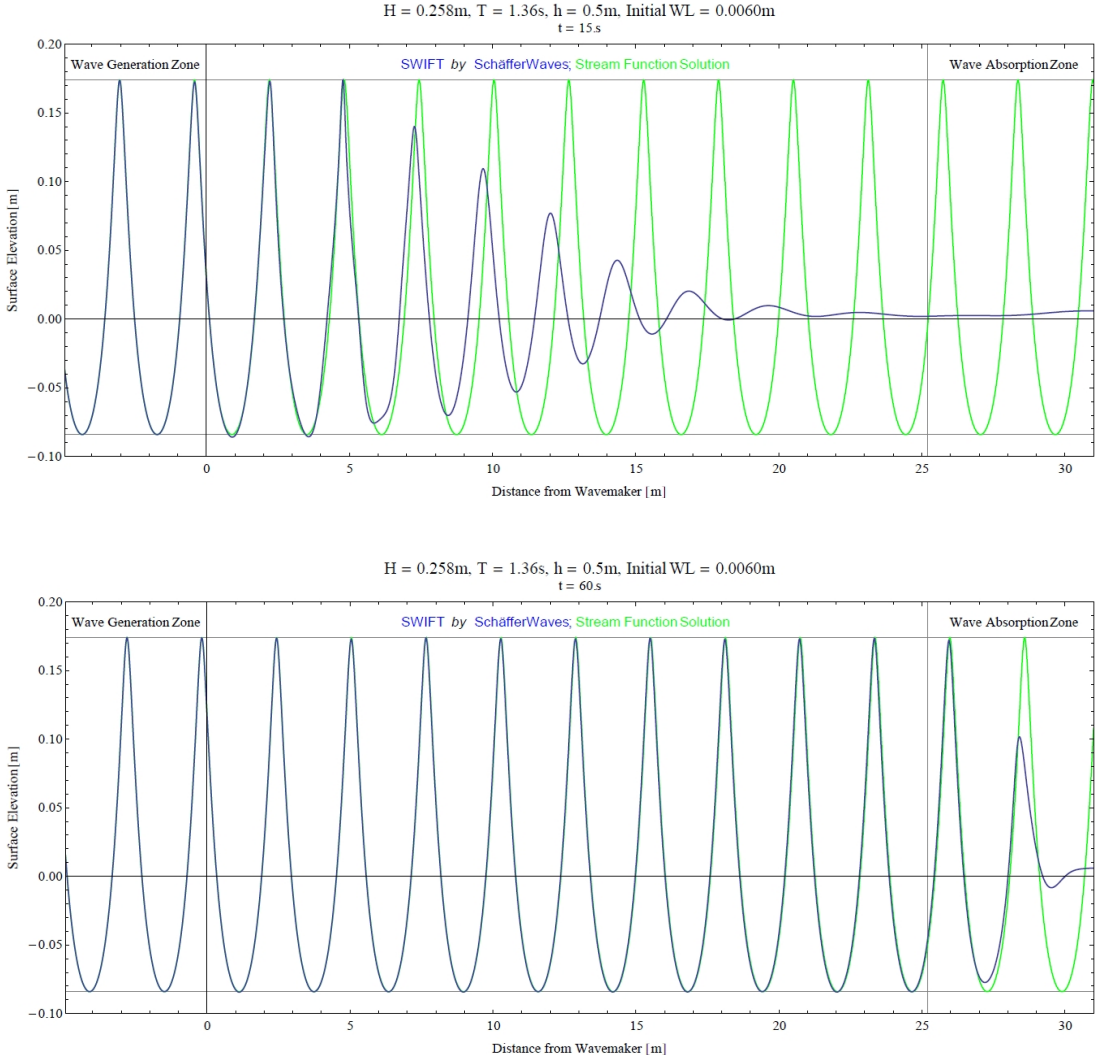

Figure 4. Snap shots of numerical surface elevation (blue) on top of the Stream Function Solution (green) at t=15s (top panel) and t=60s (bottom panel).

KINEMATICS BY POST-PROCESSING SURFACE VARIABLES FOR NONLINEAR WAVES

Prompted e.g. by applications to loads on offshore structures, a theoretical model and an associated numerical procedure for processing surface variables to obtain the internal wave field kinematics is under development. In principle the kinematics could have been determined by reworking the perturbation scheme known from the high-order spectral method (and adapted in SWIFT) to provide the still-water-level (SWL) kinematics and subsequently apply the linear convolution approach of Schäffer (2004) to obtain the kinematics field. Although this method would be valid for nonlinear waves, two issues make the approach unattractive. First, while the perturbation scheme is very accurate in the role of a Dirichlet-Neumann operator expansion (see Schäffer, 2008), it is not very accurate when twisted to provide SWL kinematics. Second, the convolution of Schäffer (2004) would only provide the kinematics below SWL. As an alternative with none of these shortcomings, an explicit boundary integral approach was taken. In short, choosing the horizontally evanescent Green's function of Schäffer (2012), but stretching the constituting vertical source-sink array, paves the way for expressing the kinematics all the way to the instantaneous water surface. Figure 5 verifies the approach for a steep regular wave with H/L = 0.13 and kh = 12. The example is the same as in Schäffer (2004, except that paper writes H/L = 0.135 although H/L = 0.13 is the correct number). For this very-deep-water case (four times deeper than what is commonly taken as deep water) a polynomial approach to the variation over the vertical tends to produce oscillatory results in the deeper parts of the water column, see Madsen et al. (2003) for a high-order approach and Madsen and Agnon (2003) for further extensions. In contrast to the polynomial approach, the present method of determining the kinematics captures the correct smooth and fast decay and as opposed to the convolution approach of Schäffer 2004, the method is valid all the way to the free surface.

Bateman et al. (2003) took a spectral approach to the computation of wave kinematics based on the surface variables, but recommended a boundary integral approach as an attractive alternative. The Green's function they mentioned in this context was the classical, fundamental solution to the Laplace equation in 3D, which is proportional to 1/r, where r is the 3D distance between source and response. The slow horizontal decay of this function, however, calls for a global computation. This is even more pronounced in 2DV, where the Green's function is proportional to log(r). The method sketched above reduces this global computation to a regional one by employing a Green's function with a practical horizontal support of just several water depths.

REFERENCES

Bateman W.J.D., Swan C., Taylor P.H., 2003. On the calculation of the water particle kinematics arising in a directionally spread wavefield, *J. of Computational Physics*,186, 70-92

Bingham, H.B., Agnon, Y., 2005. A Fourier-Boussinesq method for nonlinear water waves. *Eur. J. Mech B/Fluids*, 24, 255-274.

Dommermuth, D.G., Yue, D.K.Y., 1987. A high-order spectral method for the study of nonlinear gravity waves. *J. Fluid Mech*. 184, 267-288.

Madsen, P.A., Bingham, H.B., Schäffer, H.A., 2003. Boussinesq-type formulations for fully nonlinear and extremely dispersive water waves: derivation and analysis. *Proc. R. Soc. Lond*. A459, 1075–1104.

Madsen, P.A., Agnon, Y., 2003. Accuracy and convergence of velocity formulations for water waves in the framework of Boussinesq theory. *J. Fluid Mech*. 477,. 285–319.

Rienecker, M.M., Fenton, J.D., 1981. A Fourier approximation method for steady water waves. *J. Fluid Mech.* 104, 119–137.

Schäffer, H.A., 2004. Accurate determination of internal kinematic from numerical wave model results. *Coastal Engineering* 50, 199-211.

Schäffer, H.A., 2008. Comparison of Dirichlet–Neumann operator expansions for nonlinear surface gravity waves. *Coastal Engineering* 55, 288-294.

Schäffer, H.A., 2009. A fast convolution approach to the transformation of surface gravity waves: Linear waves in 1DH. *Coastal Engineering* 56, pp 513-533

Schäffer, H.A., 2012. Towards wave disturbance in ports computed by a deterministic convolution-type model. *Proceedings of 33rd International Conference on Coastal Engineering*, ASCE.

West, B.J., Brueckner, K.A., Janda, R.S., Milder D.M., Milton, R.L., 1987. A new numerical method for surface hydrodynamics. *J. Geophys. Res*. 92(C11), 11803-11824.

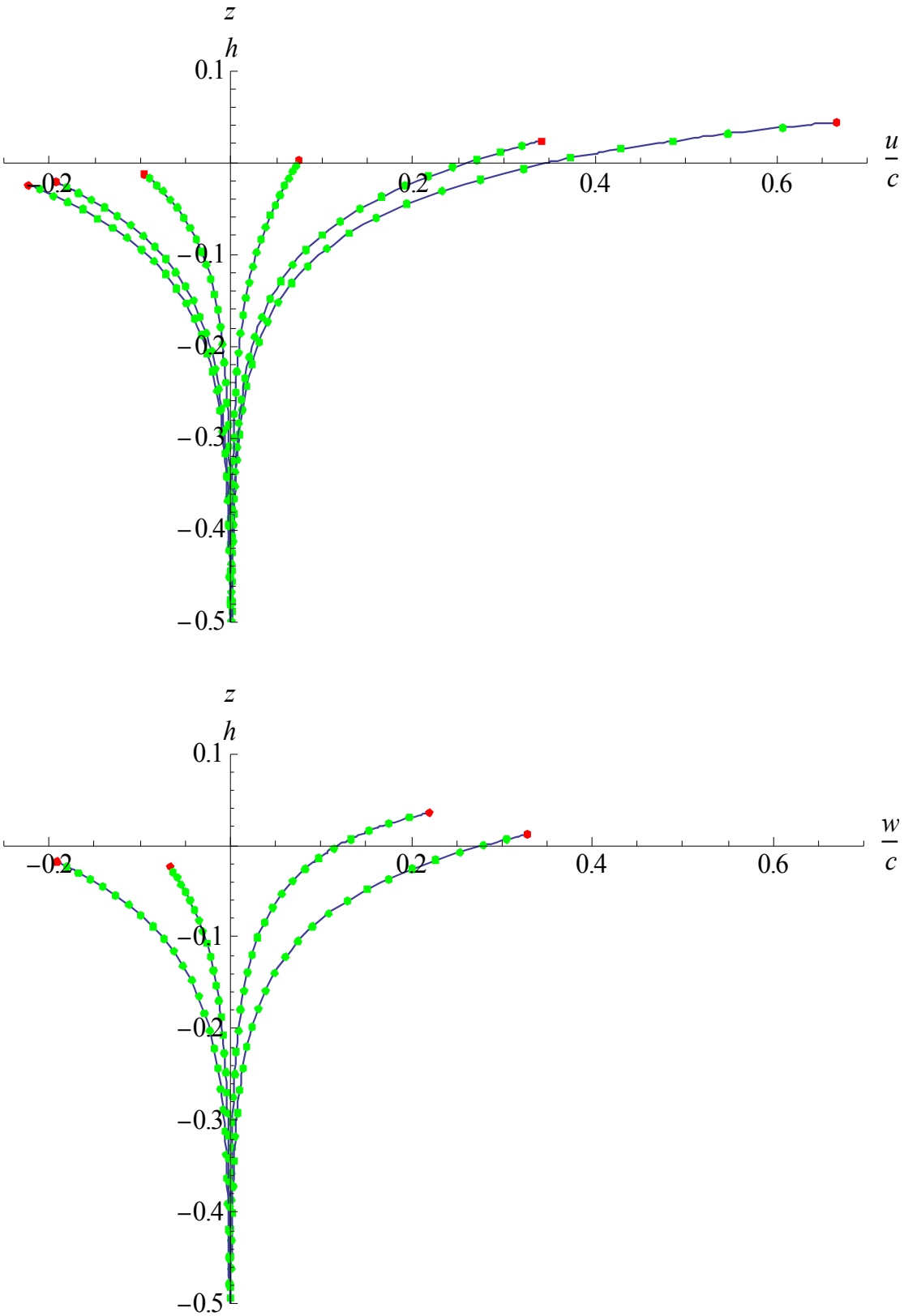

Figure 5. Kinematics computed from the surface variables (green dots, and red surface dot) on top of results of the Stream Function Solution. Top panel: horizontal velocity; Bottom panel: vertical velocity. The plots are chopped at mid depth below which the velocities vanish. The vertical axis is scaled by the depth and the particle velocities are scaled by the wave celerity. To better resolve the larger velocity gradients, the point density is increased near the surface.